Zero modes, energy gap, and edge states of anisotropic honeycomb lattice in a magnetic field

Kenta Esaki,[1] Masatoshi Sato,[1] Mahito Kohmoto,[1] and Bertrand I. Halperin[2]
[1]*Institute for Solid State Physics, University of Tokyo, Kashiwanoha 5-1-5, Kashiwa, Chiba 277-8581, Japan*
[2]*Physics Department, Harvard University, Cambridge, Massachusetts 02138, USA*
(Received 30 June 2009; revised manuscript received 10 August 2009; published 9 September 2009)

We present systematic study of zero modes and gaps by introducing effects of anisotropy of hopping integrals for a tight-binding model on the honeycomb lattice in a magnetic field. The condition for the existence of zero modes is analytically derived. From the condition, it is found that a tiny anisotropy for graphene is sufficient to open a gap around zero energy in a magnetic field. This gap behaves as a nonperturbative and exponential form as a function of the magnetic field. The nonanalytic behavior with respect to the magnetic field can be understood as tunneling effects between energy levels around two Dirac zero modes appearing in the honeycomb lattice, and an explicit form of the gap around zero energy is obtained by the Wentzel-Kramers-Brillouin method near the merging point of these Dirac zero modes. Effects of the anisotropy for the honeycomb lattices with boundaries are also studied. The condition for the existence of zero energy edge states in a magnetic field is analytically derived. On the basis of the condition, it is recognized that anisotropy of the hopping integrals induces abrupt changes in the number of zero energy edge states, which depend on the shapes of the edges sensitively.

DOI: 10.1103/PhysRevB.80.125405 PACS number(s): 71.70.Di, 73.43.−f, 81.05.Uw

I. INTRODUCTION

Recent experiments on graphene[1–5] have led to renewed interest in physical properties of electrons on the honeycomb lattice. Despite its simple structure, the honeycomb lattice provides nontrivial physical phenomena which cannot be observed in the ordinary square lattice. Among them, much attention has been paid to its peculiar dispersion. In the absence of a magnetic field, the honeycomb lattice has $E=0$ zero modes at the corners K and K' of the Brillouin zone. By treating these zero modes as Dirac fermions, the unconventional quantization of the Hall conductance observed for graphene was explained,[6–8] although the full proper theoretical treatment of the Hall conductance on the honeycomb lattice was made very recently.[9] Moreover, when the system has a boundary, there are $E=0$ edge modes localized on the boundary. The existence of the $E=0$ edge modes depends on a choice of the boundary, and for zigzag and bearded edges there occur large density of states localized on these edges at the Fermi energy due to their flat band structures.[10–20] In addition, it is suggested that the $E=0$ edge modes induce charge accumulation on these edges.[21,22]

In this paper, we study properties of these $E=0$ zero modes in the presence of anisotropy of the hopping integrals in the honeycomb lattice. Recently, the anisotropy of the hopping integrals was introduced by replacing one of the hopping integrals with a general value t (Refs. 9 and 23–28) in order to investigate the unconventional quantum Hall effects on graphene (see Fig. 1). (For $t\neq 1$, we have the anisotropic honeycomb lattice.) In Ref. 9, by using topological arguments, an algebraic expression of the quantum Hall conductance was obtained for almost all gaps including subband gaps, and it was shown that the unconventional quantization of the Hall conductance in a weak magnetic field is realized for weak t $(0<t\lesssim 1)$, while only the conventional quantization is obtained for strong t $(t>2)$. Furthermore, for the graphene case $(t=1)$, the unconventional quantization was found to persist up to the Van Hove singularity.[9,19]

The anisotropy of the hopping parameters is also known to change the peculiar dispersion mentioned above.[24–27] However, in the absence of a magnetic field, its influence is restrictive: Although a gap opens around zero energy for $t>2$, there remain two $E=0$ zero modes in the Brillouin zone for $0<t<2$.[24] Therefore, a large anisotropy is needed to change the zero mode structure. As well as the zero mode structure, that of zero energy edge states was shown to change by a large anisotropy.[28]

In this paper, it will be shown the situation is drastically changed in the presence of a magnetic field. We analytically derive the condition for the existence of zero modes in a magnetic flux $2\pi\Phi=2\pi p/q$ (p and q are mutually prime integers), and from the condition it is found that, in the limit of $q\to\infty$, zero modes exist only for $0<t\leq 1$, but a gap around zero energy opens for $t>1$. In other words, a small anisotropy $t=1+\epsilon$ $(0<\epsilon\ll 1)$ is sufficient to open a gap in the presence of a weak magnetic field.

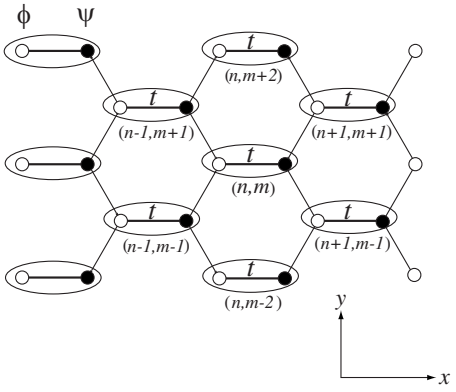

FIG. 1. The honeycomb lattice. The hopping integrals of the horizontal bonds are t, and those for the other bonds are 1. A magnetic flux $2\pi\Phi$ is applied through the unit hexagon.

For $1<t<2$, the gap around zero energy in a weak magnetic field behaves as a nonperturbative and exponential form as a function of Φ. It will be shown that this behavior is naturally explained in terms of the spontaneous breaking of supersymmetry.[29,30] In particular, an explicit form of the gap around zero energy for $t\sim 2$ is obtained by the Wentzel-Kramers-Brillouin (WKB) method. At $t=2$, the gap around zero energy in a weak magnetic field is found to make a transition from an exponential (nonperturbative) to a power-law (perturbative) behavior as a function of Φ, and for $t>2$, the energy bands in a weak magnetic field show linear dependence on Φ.

We will also show that the structure of $E=0$ edge states in the presence of a magnetic field is different from that in the absence of a magnetic field. The condition for the existence of zero energy edge states in a magnetic field is analytically derived, and it is found that the anisotropy of the hopping integrals induces abrupt changes in the number of zero energy edge states, which also sensitively depend on shapes of the edges.

The organization of this paper is as follows: in Sec. II, we present our model. The condition for the existence of zero modes in a magnetic field is analytically derived in Sec. III, both from the secular equation and from the normalizability condition of states with zero energy. On the basis of the condition for the existence of zero modes, the energy spectrum near zero energy in a weak magnetic field is systematically examined in Sec. IV. In Sec. V, zero energy edge states are analyzed, where crucial roles of the anisotropy of the hopping integrals are recognized again. Finally, we summarize our results and discuss possible experimental realization of anisotropy of the hopping integrals in Sec. VI.

II. TIGHT-BINDING MODEL ON THE HONEYCOMB LATTICE IN A MAGNETIC FIELD

Let us consider the tight-binding model on the honeycomb lattice with nearest-neighbor hopping in a magnetic field as shown in Fig. 1. By denoting wave functions on two sublattices of the honeycomb lattice as $\psi_{n,m}$ and $\phi_{n,m}$, respectively, the tight-binding model is given by

$$E\psi_{n,m} = \phi_{n+1,m-1} + e^{2i\pi\Phi n}\phi_{n+1,m+1} + t\phi_{n,m},$$

$$E\phi_{n,m} = \psi_{n-1,m+1} + e^{-2i\pi\Phi(n-1)}\psi_{n-1,m-1} + t\psi_{n,m}, \tag{1}$$

where a magnetic flux through the unit hexagon is given by $2\pi\Phi$. Here we have introduced anisotropy of the hopping integrals: the hopping integrals of the horizontal bonds are t, and those for the other bonds are 1. For simplicity, we neglect the spin degrees of freedom in the following.

III. CONDITION FOR THE EXISTENCE OF ZERO MODES

For the isotropic case ($t=1$), it was found that zero modes exist for all (rational) values of Φ.[31] We now derive the condition for the existence of zero modes in the anisotropic case.

Before examining $\Phi\neq 0$, let us first consider $\Phi=0$.[24] For $\Phi=0$, Eq. (1) gives

$$E\psi_{n,m} = \phi_{n+1,m-1} + \phi_{n+1,m+1} + t\phi_{n,m},$$

$$E\phi_{n,m} = \psi_{n-1,m+1} + \psi_{n-1,m-1} + t\psi_{n,m}. \tag{2}$$

From the Bloch's theorem, the wave functions are written as[32]

$$\psi_{n,m} = e^{ik_x n + ik_y m}\psi(\boldsymbol{k}), \quad \phi_{n,m} = e^{ik_x n + ik_y m}\phi(\boldsymbol{k}). \tag{3}$$

Substituting Eq. (3) into Eq. (2), we have

$$\mathcal{Q}(\boldsymbol{k})\begin{pmatrix}\psi(\boldsymbol{k})\\ \phi(\boldsymbol{k})\end{pmatrix} = E\begin{pmatrix}\psi(\boldsymbol{k})\\ \phi(\boldsymbol{k})\end{pmatrix}, \tag{4}$$

where $\mathcal{Q}(\boldsymbol{k})$ is given by

$$\mathcal{Q}(\boldsymbol{k}) = \begin{pmatrix}0 & \mathcal{D}(\boldsymbol{k})\\ \mathcal{D}^*(\boldsymbol{k}) & 0\end{pmatrix}, \quad \mathcal{D}(\boldsymbol{k}) = t + 2e^{ik_x}\cos k_y. \tag{5}$$

The eigenenergies E are given by

$$E = \pm|\mathcal{D}(\boldsymbol{k})| = \pm\sqrt{(t+2\cos k_x\cos k_y)^2 + 4\sin^2 k_x\cos^2 k_y}. \tag{6}$$

From Eq. (6) with $E=0$, we find two zero modes at

$$\boldsymbol{k}_0^+:(k_x^{0+},k_y^{0+}) = \left(\pi,\cos^{-1}\frac{t}{2}\right), \quad \boldsymbol{k}_0^-:(k_x^{0-},k_y^{0-}) = \left(\pi,-\cos^{-1}\frac{t}{2}\right), \tag{7}$$

for $0<t<2$. By expanding k_x and k_y around $k_x^{0\pm}$ and $k_y^{0\pm}$ in Eq. (7),

$$k_x = k_x^{0\pm} + p_x, \quad k_y = k_y^{0\pm} + p_y, \quad (|p_x|,|p_y| \ll 1), \tag{8}$$

$\mathcal{D}(\boldsymbol{k})$ is given by

$$\mathcal{D}_\pm(\boldsymbol{p}) = -itp_x \pm \sqrt{4-t^2}p_y, \tag{9}$$

where $\mathcal{D}_+(\boldsymbol{p})$ and $\mathcal{D}_-(\boldsymbol{p})$ are those near $\boldsymbol{k}_0^+$ and $\boldsymbol{k}_0^-$, respectively. From Eqs. (6) and (9), the dispersion relation of the Dirac zero mode is obtained

$$E = \pm\sqrt{t^2p_x^2 + (4-t^2)p_y^2}. \tag{10}$$

For $t=2$, the two Dirac zero modes merge into a confluent point

$$(k_x^*,k_y^*) = (\pi,0), \tag{11}$$

and for $t>2$, we have a gap around zero energy.

A. Derivation from a secular equation

Now we consider $\Phi\neq 0$. We suppose that Φ is a rational number, $\Phi=p/q$ (p and q are mutually prime integers). Since Eq. (1) has translational symmetry in the y direction, the wave functions are written as

$$\psi_{n,m} = e^{ikm}\psi_n, \quad \phi_{n,m} = e^{ikm}\phi_n, \tag{12}$$

and Eq. (1) becomes

$$E\psi_n = (e^{-ik} + e^{ik+2i\pi\Phi n})\phi_{n+1} + t\phi_n,$$

$$E\phi_n = (e^{ik} + e^{-ik-2i\pi\Phi(n-1)})\psi_{n-1} + t\psi_n. \tag{13}$$

By the gauge transformation $\psi_n \to e^{ikn}\psi_n$ and $\phi_n \to e^{ikn}\phi_n$, Eq. (13) is rewritten as

$$E\psi_n = A_n\phi_{n+1} + t\phi_n,$$

$$E\phi_n = A_{n-1}^*\psi_{n-1} + t\psi_n, \tag{14}$$

where $A_n = 1 + \exp[i(\theta_1 + 2\pi\Phi n)]$ with $\theta_1 = 2k$. Since the spectrum is found to be invariant under the transformation $\theta_1 \to \theta_1 + 2\pi/q$, we can restrict the range of θ_1 to $0 \le \theta_1 \le 2\pi/q$ without loss of generality. Moreover, in Eq. (14), (ψ_n, ϕ_n) and (ψ_{n+q}, ϕ_{n+q}) obey the same equation, thus from the Bloch's theorem, we have

$$\psi_{n+q} = \exp(iq\theta_2)\psi_n, \quad \phi_{n+q} = \exp(iq\theta_2)\phi_n, \tag{15}$$

where θ_2 satisfies $0 \le \theta_2 \le 2\pi/q$. Therefore Eq. (14) reduces to the eigenequation of a $2q \times 2q$ matrix. In the secular equation of this, all nonconstant terms containing less than q factors of $e^{i\theta_1}$ should cancel out each other since the eigenvalue has periodicity $2\pi/q$ with respect to θ_1. From this property, it is found that the secular equation is written as the following form:

$$F(E^2) + f(\theta_1, \theta_2) = 0, \tag{16}$$

where $F(E^2)$ is a qth-order polynomial of E^2 with $F(0)=0$, and it is independent of (θ_1, θ_2). The secular determinant for Eq. (14) with $E=0$ determines $f(\theta_1, \theta_2)$ as

$$f(\theta_1, \theta_2) = \left| \det \begin{pmatrix} t & A_1 & & & \\ & t & A_2 & & \\ & & \ddots & \ddots & \\ & & & t & A_{q-1} \\ e^{iq\theta_2}A_q & & & & t \end{pmatrix} \right|^2 = \left| t^q + (-1)^{q-1} e^{iq\theta_2} \prod_{n=1}^{q} A_n \right|^2$$

$$= \left| t^q + (-1)^{q+1} 2\cos\left(\frac{q}{2}\theta_1 + \frac{q+1}{2}\pi\right) e^{i[q\theta_2 + q\theta_1/2 + (q+1)\pi/2]} \right|^2. \tag{17}$$

Here we have used

$$\prod_{n=1}^{q} A_n = \prod_{n=1}^{q} [1 + e^{i(\theta_1 + 2\pi\Phi n)}]$$

$$= 1 + e^{iq\theta_1} \prod_{n=1}^{q} e^{i2\pi\Phi n}$$

$$= 1 + (-1)^{p(q+1)} e^{iq\theta_1}$$

$$= 1 + (-1)^{q+1} e^{iq\theta_1}, \tag{18}$$

which is derived from $f(\theta_1 + 2\pi/q, \theta_2) = f(\theta_1, \theta_2)$.

When t satisfies

$$0 < t \le 2^{1/q}, \tag{19}$$

the range of $f(\theta_1, \theta_2)$ is $0 \le f(\theta_1, \theta_2) \le (t^q + 2)^2$ and there exist two independent (θ_1, θ_2)'s with $f(\theta_1, \theta_2) = 0$. From the secular equation (16), we have two $E=0$ modes at these (θ_1, θ_2)'s. On the other hand, if t satisfies

$$t > 2^{1/q}, \tag{20}$$

we have $(t^q - 2)^2 \le f(\theta_1, \theta_2) \le (t^q + 2)^2$ and there is no (θ_1, θ_2) with $f(\theta_1, \theta_2) = 0$. We have a gap around zero energy in this case.

Here we note that the condition for the existence of zero modes for $\Phi = 0$, that is, $0 < t \le 2$, is reproduced by Eq. (19) with $q=1$. [When $q=1$, Eq. (1) reduces to that with $\Phi = 0$].

B. Derivation from the normalizability condition of states

In Sec. III A, we derived the condition for the existence of zero modes from the secular equation. Here, we rederive it from the normalizability condition of states with zero energy.

Let us first consider Eq. (14) with $E=0$,

$$\phi_n = -\frac{1}{t}A_n\phi_{n+1}, \quad \psi_{n+1} = -\frac{1}{t}A_n^*\psi_n. \tag{21}$$

Then for $\Phi = p/q$, Eqs. (18) and (21) lead to

$$\phi_{Nq+l} = \left(-\frac{1}{t}\right)^q \left(\prod_{n=1}^{q} A_n\right) \phi_{(N+1)q+l}$$

$$= \left(-\frac{1}{t}\right)^q [1 + (-1)^{q+1} e^{iq\theta_1}] \phi_{(N+1)q+l},$$

$$\psi_{(N+1)q+l} = \left(-\frac{1}{t}\right)^q \left(\prod_{n=1}^{q} A_n^*\right) \psi_{Nq+l}$$

$$= \left(-\frac{1}{t}\right)^q [1 + (-1)^{q+1} e^{-iq\theta_1}] \psi_{Nq+l}, \tag{22}$$

where $l = 0, 1, 2, \ldots, q-1$. Taking the absolute values of the both sides in Eq. (22), we obtain

$$|\phi_{Nq+l}| = \frac{2}{t^q} \left| \cos\left(\frac{q\theta_1}{2} + \frac{q+1}{2}\pi\right) \right| |\phi_{(N+1)q+l}|,$$

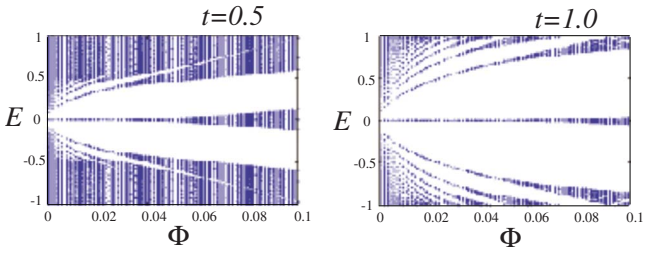

FIG. 2. (Color online) Energy bands as a function of Φ for $t=0.5$ and $t=1.0$.

$$|\psi_{(N+1)q+l}| = \frac{2}{t^q}\left|\cos\left(\frac{q\theta_1}{2}+\frac{q+1}{2}\pi\right)\right||\psi_{Nq+l}|. \quad (23)$$

For $t^q>2$, Eq. (23) gives

$$|\phi_{Nq+l}|<|\phi_{(N+1)q+l}|, \quad |\psi_{(N+1)q+l}|<|\psi_{Nq+l}|. \quad (24)$$

From (24) we see that $|\phi_n|$ diverges for $n\to\infty$, and $|\psi_n|$ diverges for $n\to-\infty$. Thus these states are not normalizable, and no relevant zero modes exist. We have a gap around $E=0$ in this case. On the other hand, for $t^q\le 2$, Eq. (23) gives

$$|\phi_{Nq+l}| = |\phi_{(N+1)q+l}|, \quad |\psi_{(N+1)q+l}| = |\psi_{Nq+l}|, \quad (25)$$

at $\theta_1=\pm\frac{2}{q}\cos^{-1}\frac{t^q}{2}+\frac{q+1}{q}\pi$. Thus there exist two zero modes for $t\le 2^{1/q}$. These results coincide with those of Sec. III A.

IV. SPECTRUM NEAR ZERO ENERGY IN A WEAK MAGNETIC FIELD

In this section, we examine the spectrum near zero energy in a weak magnetic field. Although some numerical study was presented in Ref. 23, we perform detailed analytical study here. On the basis of the condition for the existence of zero modes obtained in the previous section, we consider the following four cases separately:

(a) $0<t\le 1$, where the condition (19) is always satisfied and we have zero modes for all rational values of Φ.

(b) $1<t<2$, where zero modes disappear and a gap around $E=0$ opens for $t>2^{1/q}$.

(c) $t=2$, where one zero mode exists for $\Phi=0$.

(d) $t>2$, where no zero modes exist.

A. $0<t\le 1$

We show two examples of the energy bands as a function of Φ in Fig. 2. For $0<t\le 1$, we have zero modes for all rational values of Φ. As shown in the following, the energy bands in a weak magnetic field are well described by the continuum approximation.

In the continuum approximation, we use the Landau gauge $\mathbf{A}=(0,Bx,0)$ for a magnetic field B. Then, substitution $p_x\to\hat{p}_x$ and $p_y\to\hat{p}_y+Bx$ in Eq. (9) with $\hat{p}_x=-i\partial_x$, $\hat{p}_y=-i\partial_y$ and $B=\pi\Phi$ (see Appendix) gives the equation in a weak magnetic field as

$$\mathcal{Q}_\pm\begin{pmatrix}\psi(x,y)\\ \phi(x,y)\end{pmatrix} = E\begin{pmatrix}\psi(x,y)\\ \phi(x,y)\end{pmatrix}, \quad (26)$$

where $\mathcal{Q}_\pm$ is given by

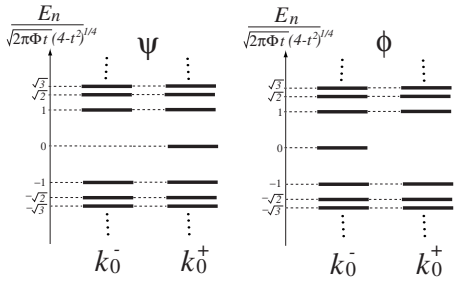

FIG. 3. Energy levels around $\boldsymbol{k}_0^+$ and $\boldsymbol{k}_0^-$.

$$\mathcal{Q}_\pm = \begin{pmatrix}0 & \mathcal{D}_\pm\\ \mathcal{D}_\pm^* & 0\end{pmatrix}, \quad \mathcal{D}_\pm = -it\hat{p}_x \pm \sqrt{4-t^2}(\hat{p}_y+\pi\Phi x). \quad (27)$$

Here, $\mathcal{D}_+$ and $\mathcal{D}_-$ are those near $\boldsymbol{k}_0^+$ and $\boldsymbol{k}_0^-$, respectively. Since $\mathcal{Q}_\pm$ and $\hat{p}_y$ commute each other, we can replace $\hat{p}_y$ with a c-number p_y. Then putting $x\to x-p_y/\pi\Phi$, we obtain

$$\mathcal{Q}_\pm\begin{pmatrix}\psi(x)\\ \phi(x)\end{pmatrix} = E\begin{pmatrix}\psi(x)\\ \phi(x)\end{pmatrix}, \quad (28)$$

where

$$\mathcal{Q}_\pm = \begin{pmatrix}0 & \mathcal{D}_\pm\\ \mathcal{D}_\pm^* & 0\end{pmatrix}, \quad \mathcal{D}_\pm = -it\hat{p}_x \pm \sqrt{4-t^2}\pi\Phi x. \quad (29)$$

From Eqs. (28) and (29), the following equation is obtained:

$$\mathcal{H}_\pm\begin{pmatrix}\psi(x)\\ \phi(x)\end{pmatrix} = E^2\begin{pmatrix}\psi(x)\\ \phi(x)\end{pmatrix}, \quad (30)$$

where

$$\mathcal{H}_\pm = \mathcal{Q}_\pm^2 = \begin{pmatrix}\mathcal{D}_\pm\mathcal{D}_\pm^* & 0\\ 0 & \mathcal{D}_\pm^*\mathcal{D}_\pm\end{pmatrix}. \quad (31)$$

Therefore, we have

$$[t^2\hat{p}_x^2+(4-t^2)\pi^2\Phi^2x^2-t\sqrt{4-t^2}\pi\Phi\sigma_z]\begin{pmatrix}\psi(x)\\ \phi(x)\end{pmatrix} = E^2\begin{pmatrix}\psi(x)\\ \phi(x)\end{pmatrix}, \quad (32)$$

around $\boldsymbol{k}_0^+$, and

$$[t^2\hat{p}_x^2+(4-t^2)\pi^2\Phi^2x^2+t\sqrt{4-t^2}\pi\Phi\sigma_z]\begin{pmatrix}\psi(x)\\ \phi(x)\end{pmatrix} = E^2\begin{pmatrix}\psi(x)\\ \phi(x)\end{pmatrix}, \quad (33)$$

around $\boldsymbol{k}_0^-$, where σ_z is the z component of the Pauli matrix. Since the equations for ψ in Eqs. (32) and (33) essentially coincide with those for harmonic oscillators, the energy level for ψ around $\boldsymbol{k}_0^+$ is given by

$$E_n = \pm\sqrt{2\pi\Phi t}(4-t^2)^{1/4}\sqrt{n}, \quad (n=0,1,2,\ldots), \quad (34)$$

and that around $\boldsymbol{k}_0^-$ is given by

$$E_n = \pm\sqrt{2\pi\Phi t}(4-t^2)^{1/4}\sqrt{n+1}, \quad (n=0,1,2,\ldots). \quad (35)$$

In a similar manner, the energy levels for ϕ around $\boldsymbol{k}_0^+$ and $\boldsymbol{k}_0^-$ are given by

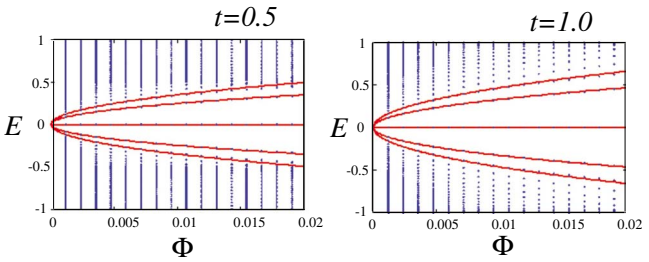

FIG. 4. (Color online) A closer look of Fig. 2 in a weak magnetic field region. The energy levels (34) and (35) [or (36) and (37)] are also shown by the red lines.

$$E_n = \pm \sqrt{2\pi\Phi t}(4-t^2)^{1/4}\sqrt{n+1}, \quad (n=0,1,2,\ldots), \quad (36)$$

and

$$E_n = \pm \sqrt{2\pi\Phi t}(4-t^2)^{1/4}\sqrt{n}, \quad (n=0,1,2,\ldots), \quad (37)$$

respectively. We show the energy levels around $\boldsymbol{k}_0^+$ and $\boldsymbol{k}_0^-$ in Fig. 3. As illustrated in Fig. 4, the energy bands for $0<t\leq 1$ come to be well fitted by Eqs. (34) and (35) [or Eqs. (36) and (37)] in a weak magnetic field.

B. $1<t<2$

For $1<t<2$, a gap around $E=0$ opens for $t>2^{1/q}$. This implies that *in a weak magnetic field* $(q\gg 1)$, *a gap around* $E=0$ opens by a tiny distortion of graphene, $t=1+\epsilon$ $(0<\epsilon\ll 1)$. Since we do not have $E=0$ states, the expressions (34) and (37) need to be modified. We show two examples of energy bands as a function of Φ for $1<t<2$ in Fig. 5.

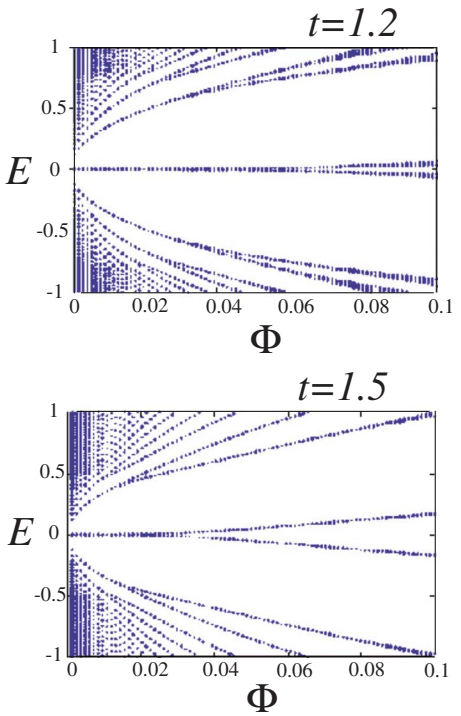

FIG. 5. (Color online) Energy bands as a function of Φ for $t=1.2$ and $t=1.5$.

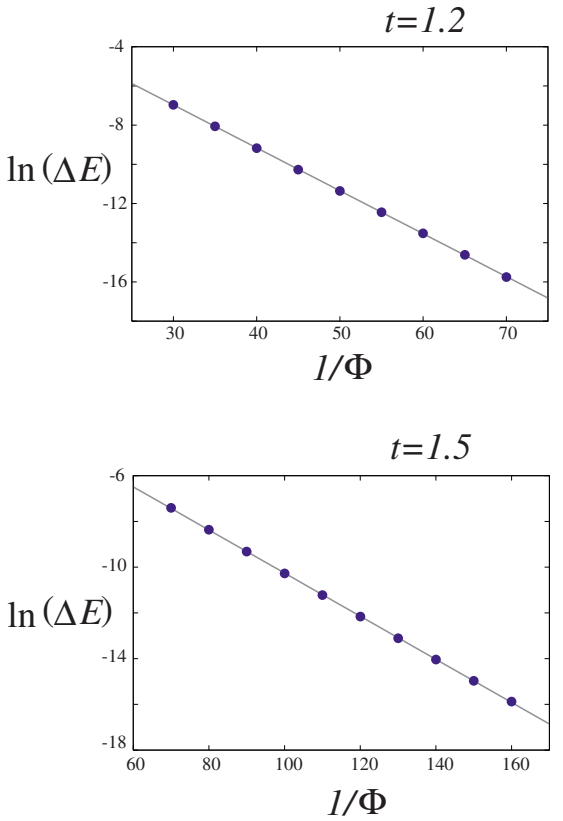

FIG. 6. (Color online) The natural logarithm of the gap around $E=0$ as a function of $1/\Phi$ for $t=1.2$ and $t=1.5$. The slope of the fitting line gives $-\alpha$.

Let us focus on the gap around $E=0$. In order to see how it behaves, we plot the natural logarithm of the gap ΔE around $E=0$ as a function of $1/\Phi$ in Fig. 6. From this, we find that it behaves as

$$\Delta E \sim \exp(-\alpha/\Phi). \quad (38)$$

The values of α are obtained from Fig. 6 as $\alpha\sim 0.22$ and 0.094 for $t=1.2$ and 1.5, respectively.

The nonanalytic behavior (38) can be understood as breaking of supersymmetry[29,30,33] in our model. The operator $\mathcal{Q}_\pm$ transforms ψ to ϕ and vice versa, which is seen from Eqs. (28) and (29). By identifying $\mathcal{Q}_\pm$ with generators of supersymmetry, $\mathcal{H}_\pm$ in Eq. (30) can be considered as supersymmetric Hamiltonians, $\mathcal{H}_\pm=\mathcal{Q}_\pm^2$ (ϕ is "boson," and ψ is "fermion"). Due to the supersymmetry, there is no perturbative (or power-law) correction with respect to Φ for the $E=0$ states. However, tunneling effects break the supersymmetry spontaneously and the nonperturbative correction (38) appears as a gap around $E=0$.

When two Dirac zero modes at $\Phi=0$ are close to each other in the momentum space, namely, $t\sim 2$, the gap around $E=0$ can be estimated by the WKB method. For $t\sim 2$, the two Dirac zero modes at $\Phi=0$ are located at Eq. (7) with

$$\cos^{-1}\frac{t}{2} \sim \sqrt{2-t} \equiv G, \quad (39)$$

and for $t=2$, they merge into a confluent point (11). For $t\sim 2$, it is convenient to expand k_x and k_y around the confluent point (11) instead of $\boldsymbol{k}_0^+$ or $\boldsymbol{k}_0^-$

$$k_x = k_x^* + p_x = \pi + p_x, \quad k_y = k_y^* + p_y = p_y, \quad (|p_x|, |p_y| \ll 1). \tag{40}$$

Then $\mathcal{D}(\boldsymbol{k})$ in Eq. (5) is given by

$$\mathcal{D}(\boldsymbol{k}) = -2ip_x + p_y^2 - G^2. \tag{41}$$

In a weak Φ, we can use the continuum approximation. We use the Landau gauge $\mathbf{A}=(0,Bx,0)$ for a magnetic field B. Then, substitution $p_x \to \hat{p}_x$ and $p_y \to \hat{p}_y + Bx$ in Eq. (41) with $\hat{p}_x = -i\partial_x$, $\hat{p}_y = -i\partial_y$ and $B = \pi\Phi$ (see Appendix) gives the following equation:

$$\mathcal{Q}\begin{pmatrix} \psi(x,y) \\ \phi(x,y) \end{pmatrix} = E\begin{pmatrix} \psi(x,y) \\ \phi(x,y) \end{pmatrix}, \tag{42}$$

where $\mathcal{Q}$ is given by

$$\mathcal{Q} = \begin{pmatrix} 0 & \mathcal{D} \\ \mathcal{D}^* & 0 \end{pmatrix}, \quad \mathcal{D} = -2i\hat{p}_x + (\hat{p}_y + \pi\Phi x)^2 - G^2. \tag{43}$$

In a similar manner as Sec. IV A, we replace $\hat{p}_y$ with a c-number p_y and put $x \to x - p_y/\pi\Phi$. Then we obtain

$$\mathcal{Q}\begin{pmatrix} \psi(x) \\ \phi(x) \end{pmatrix} = E\begin{pmatrix} \psi(x) \\ \phi(x) \end{pmatrix}, \tag{44}$$

where $\mathcal{Q}$ is given by

$$\mathcal{Q} = \begin{pmatrix} 0 & \mathcal{D} \\ \mathcal{D}^* & 0 \end{pmatrix}, \quad \mathcal{D} = -2i\hat{p}_x + \pi^2\Phi^2 x^2 - G^2. \tag{45}$$

Identifying $\mathcal{Q}$ with a generator of supersymmetry, we have the supersymmetric Hamiltonian $\mathcal{H} = \mathcal{Q}^2$, which satisfies

$$\mathcal{H}\begin{pmatrix} \psi(x) \\ \phi(x) \end{pmatrix} = E^2\begin{pmatrix} \psi(x) \\ \phi(x) \end{pmatrix}. \tag{46}$$

By using the following variable q,

$$x + \frac{G}{\pi\Phi} = q\sqrt{\frac{1}{\pi G\Phi}}, \tag{47}$$

Eq. (46) can be rewritten as

$$\left[-\frac{1}{2}\frac{d^2}{dq^2} + \frac{1}{2}q^2(1-gq)^2 - \left(gq - \frac{1}{2}\right)\sigma_z\right]\begin{pmatrix} \psi(q) \\ \phi(q) \end{pmatrix} = \mathcal{E}\begin{pmatrix} \psi(q) \\ \phi(q) \end{pmatrix}, \tag{48}$$

with

$$g = \frac{1}{2G}\sqrt{\frac{\pi\Phi}{G}}, \quad \mathcal{E} = \frac{1}{8\pi\Phi G}E^2. \tag{49}$$

Therefore, the potential terms for $\psi(x)$ and $\phi(x)$ are given by

$$V_+(q) = \frac{1}{2}q^2(1-gq)^2 - gq, \tag{50}$$

and

$$V_-(q) = \frac{1}{2}q^2(1-gq)^2 + gq, \tag{51}$$

respectively (see Fig. 7).

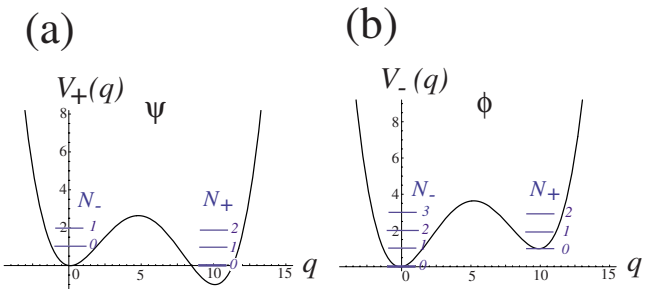

FIG. 7. (Color online) The asymmetric double-well potential (a) given by Eq. (50) with $g=0.1$, and (b) given by Eq. (51) with $g=0.1$. Energy levels around $q=0$ and $q=1/g$ are also shown.

In the leading order of g, the potentials (50) and (51) are well approximated by the harmonic oscillator around $q=0$ and $q=1/g$. Around $q=0$, Eq. (48) becomes

$$\left[-\frac{1}{2}\frac{d^2}{dq^2} + \frac{1}{2}q^2 + \frac{1}{2}\sigma_z\right]\begin{pmatrix} \psi(q) \\ \phi(q) \end{pmatrix} = \mathcal{E}\begin{pmatrix} \psi(q) \\ \phi(q) \end{pmatrix}, \tag{52}$$

and around $q=1/g$, Eq. (48) becomes

$$\left[-\frac{1}{2}\frac{d^2}{dq^2} + \frac{1}{2}\left(q - \frac{1}{g}\right)^2 - \frac{1}{2}\sigma_z\right]\begin{pmatrix} \psi(q) \\ \phi(q) \end{pmatrix} = \mathcal{E}\begin{pmatrix} \psi(q) \\ \phi(q) \end{pmatrix}. \tag{53}$$

Therefore, the energy levels for ψ around $q=1/g$ and $q=0$ are given by

$$\mathcal{E}_{N_+} = N_+, \quad (N_+ = 0,1,2,\ldots), \tag{54}$$

and

$$\mathcal{E}_{N_-} = N_- + 1, \quad (N_- = 0,1,2,\ldots), \tag{55}$$

respectively, and those for ϕ around $q=1/g$ and $q=0$ are given by

$$\mathcal{E}_{N_+} = N_+ + 1, \quad (N_+ = 0,1,2,\ldots), \tag{56}$$

and

$$\mathcal{E}_{N_-} = N_-, \quad (N_- = 0,1,2,\ldots), \tag{57}$$

respectively.

Now take into account tunneling effects between the energy levels around $q=0$ and $q=1/g$. The tunneling effects can be estimated by the WKB method presented in Appendix D of Ref. 33. Here we consider only the equation for $\psi(q)$ since the equation for $\phi(q)$ gives the same result. The solution of Eq. (52) which vanishes for $q \to -\infty$ is given by

$$\psi(q) = AD_\nu(-\sqrt{2}q), \tag{58}$$

where $\nu = \mathcal{E} - 1$, A is a constant, and D_ν the parabolic cylinder function.[34] The solution of Eq. (53) which vanishes for $q \to \infty$ is

$$\psi(q) = \tilde{A}D_{\nu+1}[\sqrt{2}(q - 1/g)], \tag{59}$$

where $\tilde{A}$ is a constant. We connect these solutions (58) and (59) with that in the forbidden region. In the forbidden re-

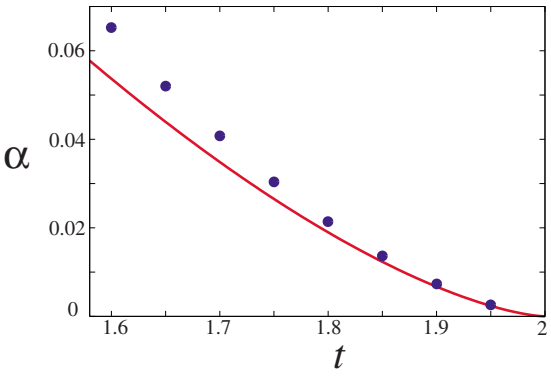

FIG. 8. (Color online) α as a function of t, where those obtained from numerical calculations and the WKB analysis are shown by points and the line, respectively.

gion, the usual semiclassical expression for the wave function is available

$$\psi(q) = \frac{C_1}{\sqrt{k(q)}}\exp\left(-\int_{q_1}^{q} k(x)dx\right) + \frac{C_2}{\sqrt{k(q)}}\exp\left(\int_{q_1}^{q} k(x)dx\right), \tag{60}$$

where $k(q)=\sqrt{2(V_+(q)-\mathcal{E})}$ with $V_+(q)$ in Eq. (50), q_i $(i=1,2)$ are the turning points, $V_+(q_i)=\mathcal{E}$, and C_i $(i=1,2)$ are constants. Connecting Eq. (58) with Eq. (60), and Eq. (59) with Eq. (60), we obtain

$$\gamma^2\left(-\frac{2}{g^2}\right)^{2\mathcal{E}-1}\Gamma(1-\mathcal{E})\Gamma(-\mathcal{E}) = 1, \quad \gamma = \frac{e^{-1/6g^2}}{g\pi^{1/2}}. \tag{61}$$

For $\mathcal{E}$ near zero energy $(\mathcal{E}\ll 1)$, we have

$$\left(-\frac{2}{g^2}\right)^{2\mathcal{E}-1} \simeq -\frac{g^2}{2}, \quad \Gamma(1-\mathcal{E}) \simeq 1, \quad \Gamma(-\mathcal{E}) \simeq -\frac{1}{\mathcal{E}}, \tag{62}$$

thus the solution of Eq. (61) for $g\ll 1$ is obtained as

$$\mathcal{E}\left(=\frac{1}{8\pi\Phi G}E^2\right) = \gamma^2\frac{g^2}{2}. \tag{63}$$

This implies that the gap around $E=0$ is given by

$$\Delta E = 4\sqrt{\Phi G}\exp\left(-\frac{2G^3}{3\pi\Phi}\right), \tag{64}$$

and the exponent α in Eq. (38) is given by

$$\alpha = \frac{2}{3\pi}G^3 = \frac{2}{3\pi}(2-t)^{3/2} \equiv \alpha_{\mathrm{WKB}}, \quad (0<2-t\ll 1). \tag{65}$$

Now we compare Eq. (65) with those obtained numerically for a small Φ. In Fig. 8, we show α as a function of t, and in Table I, we list them. The relative discrepancy

TABLE I. α for several t obtained from numerical calculations and the WKB analysis. The relative discrepancies between them, δ, are also shown.

t	α	α_{WKB}	δ
1.6	6.523×10^{-2}	5.368×10^{-2}	0.177
1.65	5.198×10^{-2}	4.394×10^{-2}	0.155
1.7	4.076×10^{-2}	3.487×10^{-2}	0.145
1.75	3.042×10^{-2}	2.653×10^{-2}	0.128
1.8	2.140×10^{-2}	1.898×10^{-2}	0.113
1.85	1.369×10^{-2}	1.233×10^{-2}	0.0993
1.9	7.294×10^{-3}	6.711×10^{-3}	0.0799
1.95	2.555×10^{-3}	2.373×10^{-3}	0.0712

$$\delta \equiv \left|\frac{\alpha_{\mathrm{WKB}}-\alpha}{\alpha}\right|, \tag{66}$$

decreases as t approaches 2. This is because the neglected terms $O(p_y^4)$ in Eq. (41) come to be smaller and smaller as t approaches 2.

C. $t=2$

At $t=2$, the two Dirac zero modes at $\Phi=0$ merge into the confluent point (11). As a consequence, a gap around $E=0$ in a weak magnetic field makes a transition from an exponential (nonperturbative) to a power-law (perturbative) behavior as a function of Φ.

In Fig. 9(a), we show the energy bands as a function of Φ for $t=2.0$. We show the three lowest bands in $E\geq 0$ in the log-log scale for weak magnetic field in Fig. 9(b). We fit our data by

$$E \sim \Phi^{\kappa}. \tag{67}$$

For $t=2.0$, we obtain the exponent κ as $\kappa\sim 0.66$, 0.65, and 0.65 for the lowest, the second lowest, and the third lowest bands in $E\geq 0$, respectively. Thus for $t=2.0$ we have a power-law behavior $E\sim\pm\Phi^{2/3}$.

The behavior $E\sim\pm\Phi^{2/3}$ is derived analytically from a particular dispersion relation at $t=2$ for $\Phi=0$.[25] For $\Phi=0$, Eqs. (6) and (41) with $G=0$ give

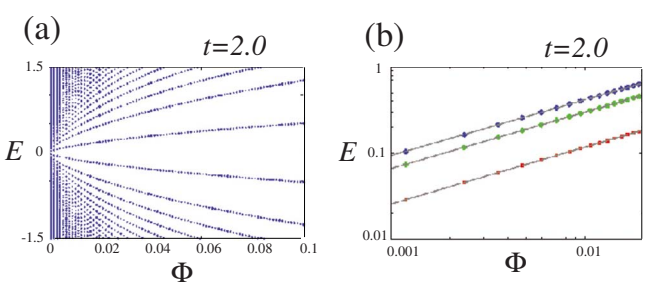

FIG. 9. (Color online) (a) Energy bands as a function of Φ for $t=2.0$. (b) The three lowest bands in $E\geq 0$ in the log-log scale.

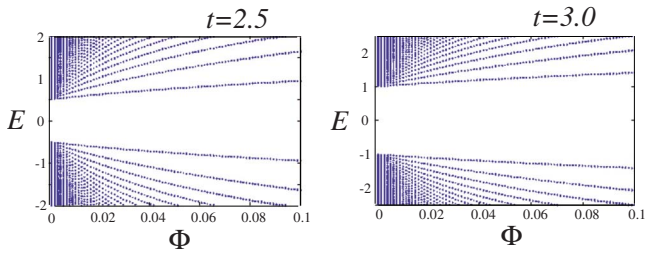

FIG. 10. (Color online) Energy bands as a function of Φ for $t=2.5$ and $t=3.0$.

$$E = \pm \sqrt{4p_x^2 + p_y^4}, \tag{68}$$

which is linear in one direction and quadratic in the other. The exponent κ is obtained from $S(E) \sim \Phi$, where $S(E)$ is the area surrounded by an orbit of energy E in the momentum space.[25] From Eq. (68), we have

$$S(E) = \frac{\Gamma(1/4)^2}{3\sqrt{2\pi}}|E|^{3/2}, \tag{69}$$

thus $E \sim \pm \Phi^{2/3}$.

D. $t>2$

For $t>2$, we do not have zero modes but have a gap around $E=0$. In Fig. 10, we show two examples of the energy bands as a function of Φ for $t>2$.

Let us study behavior of energy bands in a weak magnetic field by the continuum approximation. For $\Phi=0$, we expand k_x and k_y around $(k_x,k_y)=(\pi,0)$,

$$k_x = \pi + p_x, \quad k_y = p_y, \quad (|p_x|,|p_y| \ll 1), \tag{70}$$

then Eq. (6) gives

$$E = \pm \sqrt{E_g^2 + 2tp_x^2 + 2(t-2)p_y^2}, \quad E_g = t-2. \tag{71}$$

Thus for small $|p_x|$ and $|p_y|$ ($|p_x|,|p_y| \ll E_g$), Eq. (71) is written as

$$E = \pm \left(E_g + \frac{t}{t-2}p_x^2 + p_y^2 \right), \tag{72}$$

which is quadratic in both p_x and p_y. In the continuum approximation, we put $p_x \to \hat{p}_x$ and $p_y \to \hat{p}_y + Bx$ with $\hat{p}_x = -i\partial_x$, $\hat{p}_y = -i\partial_y$ and $B = \pi\Phi$. Then we have

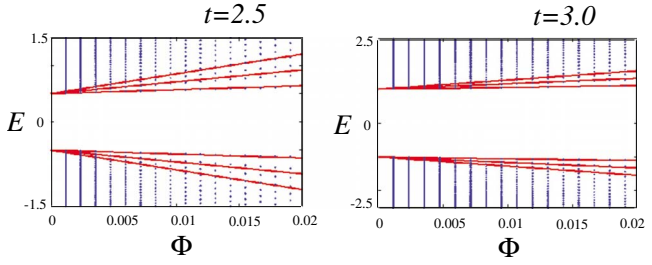

FIG. 11. (Color online) A closer look of Fig. 10 in a weak magnetic field region. The expressions (73) for $n=0,1,2$ are also shown by the red lines.

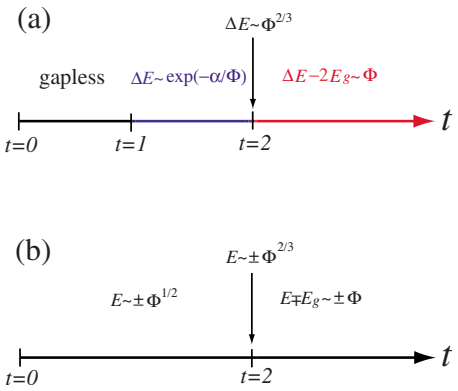

FIG. 12. (Color online) (a) Behavior of a gap ΔE around $E=0$ as a function of t in a weak magnetic field. (The nearest bands to $E=0$ show the same behavior as ΔE). (b) Behavior of the other energy bands for $E \approx 0$ as a function of t in a weak magnetic field.

$$E = \pm E_g \left[1 + 2\pi\sqrt{t}\left(n + \frac{1}{2} \right) \frac{\Phi}{(t-2)^{3/2}} \right], \quad (n = 0,1,2,\ldots), \tag{73}$$

where we have neglected higher order corrections of $O((\frac{2\pi\sqrt{t}(n+1/2)\Phi}{(t-2)^{3/2}})^2)$. The energy bands in the weak magnetic field limit ($\Phi \ll \frac{(t-2)^{3/2}}{2\pi\sqrt{t}(n+1/2)}$) are well approximated by Eq. (73), which is seen in Fig. 11. We note that, for $t \sim 2$, the neglected higher order corrections of $O((\frac{2\pi\sqrt{t}(n+1/2)\Phi}{(t-2)^{3/2}})^2)$ cannot be neglected. However, they become small for $t \gg 2$, and the energy bands in a weak magnetic field are well fitted by Eq. (73). This result is consistent with the fact that the honeycomb lattice becomes equivalent to the square lattice for $t \gg 2$.[9,26]

We summarize our results of this section in Fig. 12.

V. $E=0$ EDGE STATES IN ANISOTROPIC HONEYCOMB LATTICE

In this section, we examine $E=0$ edge states. The condition for the existence of zero energy edge states in a mag-

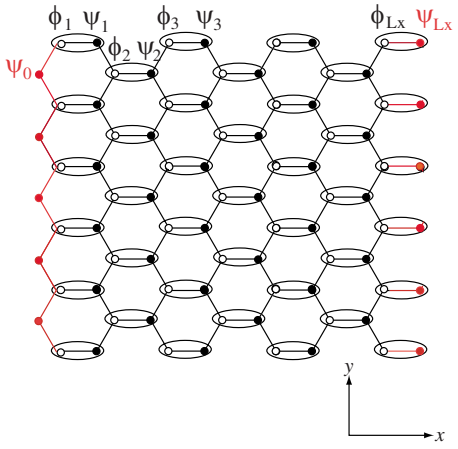

FIG. 13. (Color online) Honeycomb lattices with zigzag and bearded edges ($L_x=7$). The left and the right edges are the zigzag and the bearded edges, respectively.

netic field is analytically derived. On the basis of it, it turns out that the anisotropy of the hopping integrals induces abrupt changes in the number of zero energy edge states, which depend on the shapes of the edges sensitively.

In order to see this, we focus on the honeycomb lattices with zigzag and bearded edges as shown in Fig. 13. For these lattices, we have edges along the y direction. Let us impose the periodic boundary condition along the y direction

$$\psi_{n,m+2L_y} = \psi_{n,m}, \quad \phi_{n,m+2L_y} = \phi_{n,m}, \tag{74}$$

where an integer L_y denotes the circumference of the cylinder. Then one can write

$$\psi_{n,m} = \exp\left(i\frac{k_y}{2}m\right)\psi_n, \quad \phi_{n,m} = \exp\left(i\frac{k_y}{2}m\right)\phi_n. \tag{75}$$

Let us focus on $E=0$ states. In the same manner as Sec. III B, for $E=0$ and $\Phi=p/q$ with coprime integers p and q, the amplitudes of wave functions separated by a distance of q are found to satisfy

$$|\psi_{(N+1)q+l}| = r|\psi_{Nq+l}|, \quad |\phi_{Nq+l}| = r|\phi_{(N+1)q+l}|,$$

$$(l = 0,1,2,\ldots,q-1), \tag{76}$$

with

$$r \equiv \frac{2}{t^q}\left|\cos\left(q\frac{k_y}{2} + \frac{q+1}{2}\pi\right)\right|. \tag{77}$$

From Eq. (76), we have

$$|\psi_{Nq+l}| = r^N|\psi_l|, \quad |\phi_l| = r^N|\phi_{Nq+l}|. \tag{78}$$

The boundary conditions for the zigzag and the bearded edges are given by

$$\phi_0 = 0, \quad \phi_{Lx+1} = 0, \tag{79}$$

respectively. These boundary conditions give $\phi_n=0$ for all n, thus we consider only ψ_n in the following.

Suppose that L_x is large enough: $L_x \gg q$. Then from Eq. (78), if $r<1$ ($r>1$) we have $E=0$ states on the zigzag edge (bearded edge). For $t>2^{1/q}$, $r<1$ is satisfied for all values of k_y, but $r>1$ is not satisfied for any values of k_y. Thus we have $E=0$ states localized on the zigzag edge for all values of k_y, but we do not have $E=0$ states localized on the bearded edge for any values of k_y. For $t<2^{1/q}$, $E=0$ edge states exist both on the zigzag and the bearded edge. The total width $d_{\text{zigzag}}(t,q)$ of the region of k_y which gives $E=0$ states on the zigzag edge is given by

$$d_{\text{zigzag}}(t,q) = 2\left(\pi - 2\cos^{-1}\frac{t^q}{2}\right), \tag{80}$$

and that for the bearded edge, $d_{\text{bearded}}(t,q)$, is given by

$$d_{\text{bearded}}(t,q) = 2\pi - d_{\text{zigzag}}(t,q) = 4\cos^{-1}\frac{t^q}{2}. \tag{81}$$

For a fixed value of Φ, d_{zigzag} (d_{bearded}) increases (decreases) as t increases in the region of $0<t<2^{1/q}$. At $t=2^{1/q}$, d_{zigzag} covers the whole region of k_y, and d_{bearded} vanishes. For $t>2^{1/q}$, we have $E=0$ edge states on the zigzag edges for all values of k_y. We show examples of the energy spectra of honeycomb lattices with zigzag and bearded edges in Figs. 14 and 15.

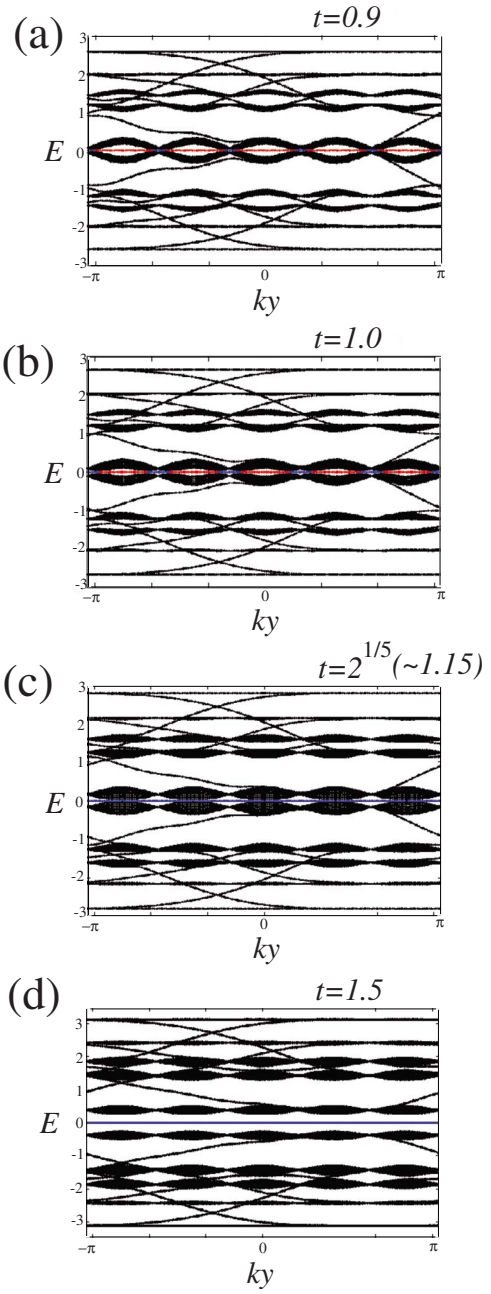

FIG. 14. (Color online) Energy spectra of honeycomb lattices with zigzag and bearded edges for $\Phi=1/5$ and $L_x=50$. (a) $t=0.9$, (b) $t=1.0$, (c) $t=2^{1/5}(\sim 1.15)$ (d) $t=1.5$. The $E=0$ edge states localized on the zigzag edges are on the blue lines, and those localized on the bearded edges are on the red lines.

Effects of the anisotropy of the hopping integrals are evident in a weak magnetic field, $\Phi \ll 1$ ($q \gg 1$). For $t=1$, d_{zigzag} and d_{bearded} do not depend on the magnetic field, and are given by $d_{\text{zigzag}}=\frac{2\pi}{3}$ and $d_{\text{bearded}}=\frac{4\pi}{3}$, respectively. However, for $t<1$, d_{zigzag} decreases toward 0 and d_{bearded} increases toward 2π as q increases. In contrast, for $t>1$, d_{zigzag} (d_{bearded}) increases (decreases) as q increases and reaches 2π (0) at $q=\ln 2/\ln t$. Note that even in a small anisotropy, d_{zigzag} and

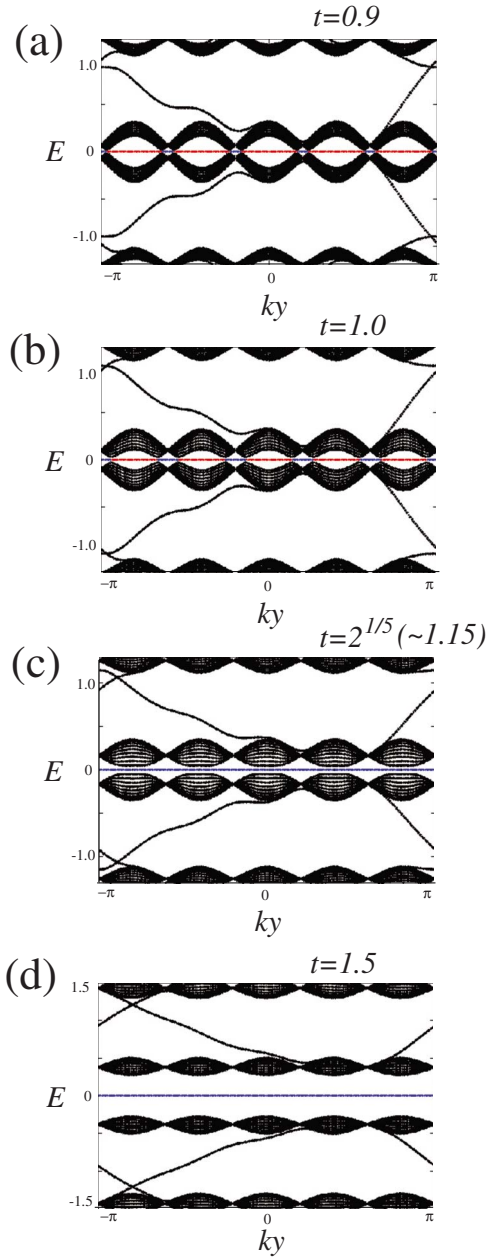

FIG. 15. (Color online) A closer look of Fig. 14 at $E \approx 0$.

d_{bearded} change abruptly in a weak magnetic field ($q \gg 1$).

Instead of d_{zigzag} and d_{bearded}, we also consider the integrated charge density I_n for $E=0$ edge states[21,22]

$$I_n = \int |\psi_n(k_y)|^2 dk_y, \tag{82}$$

where the normalization condition is imposed on $\psi_n(k_y)$,

$$\sum_{n=0}^{L_x} |\psi_n(k_y)|^2 = 1. \tag{83}$$

To characterize the numbers of the states localized on the edges, we introduce the following quantities:

$$N_{\text{zigzag}} = \sum_{n=0}^{q-1} I_n, \quad N_{\text{bearded}} = \sum_{n=L_x-q+1}^{L_x} I_n. \tag{84}$$

For $r<1$, only the zigzag edge has $E=0$ modes, and N_{zigzag} is evaluated as

$$N_{\text{zigzag}} = \int \left(1 - \frac{2}{t^{2q}}\right) dk_y + (-1)^q \frac{2}{t^{2q}} \int \cos(qk_y) dk_y, \tag{85}$$

where the domain of the integration is restricted to those k_y with $r<1$. Here we have used the relation derived from Eqs. (78) and (83)

$$\sum_{j=0}^{\lfloor (L_x+1)/q \rfloor - 1} r^{2j} \sum_{n=0}^{q-1} |\psi_n(k_y)|^2 + O(r^{2L_x/q}) = 1, \tag{86}$$

where $O(r^{2L_x/q})$ corrections can be neglected since $r<1$ and $L_x \gg q$. ($\lfloor x \rfloor$ denotes the integer part of x.) Eq. (86) is rewritten as

$$\sum_{n=0}^{q-1} |\psi_n(k_y)|^2 = 1 - r^2 + O(r^{2L_x/q}), \tag{87}$$

then substituting this into the first equation in Eq. (84) and using Eq. (77), we obtain Eq. (85). On the other hand, for $r>1$, we have $E=0$ modes only on the bearded edge, and N_{bearded} is given by

$$N_{\text{bearded}} = \int dk_y - \frac{t^{2q}}{4} \int \frac{1}{\cos^2\left(q\frac{k_y}{2} + \frac{q+1}{2}\pi\right)} dk_y, \tag{88}$$

where the domain of the integration is restricted to those k_y with $r>1$. Here we have used the relation

$$\sum_{n=L_x-q+1}^{L_x} |\psi_n(k_y)|^2 = 1 - r^{-2} + O(r^{-2L_x/q}), \tag{89}$$

which is derived from Eqs. (78) and (83) in a similar manner as Eq. (87).

Let us now evaluate N_{zigzag} and N_{bearded} from Eqs. (85) and (88). For $t>2^{1/q}$, $r<1$ is realized for all values of k_y as shown above. Therefore,

$$N_{\text{zigzag}} = \int_0^{2\pi} \left(1 - \frac{2}{t^{2q}}\right) dk_y + (-1)^q \frac{2}{t^{2q}} \int_0^{2\pi} \cos(qk_y) dk_y$$
$$= 2\pi \left(1 - \frac{2}{t^{2q}}\right),$$

$$N_{\text{bearded}} = 0. \tag{90}$$

For $t<2^{1/q}$, either $r>1$ or $r<1$ is realized by a suitable choice of k_y. Thus both N_{zigzag} and N_{bearded} become nonzero as,

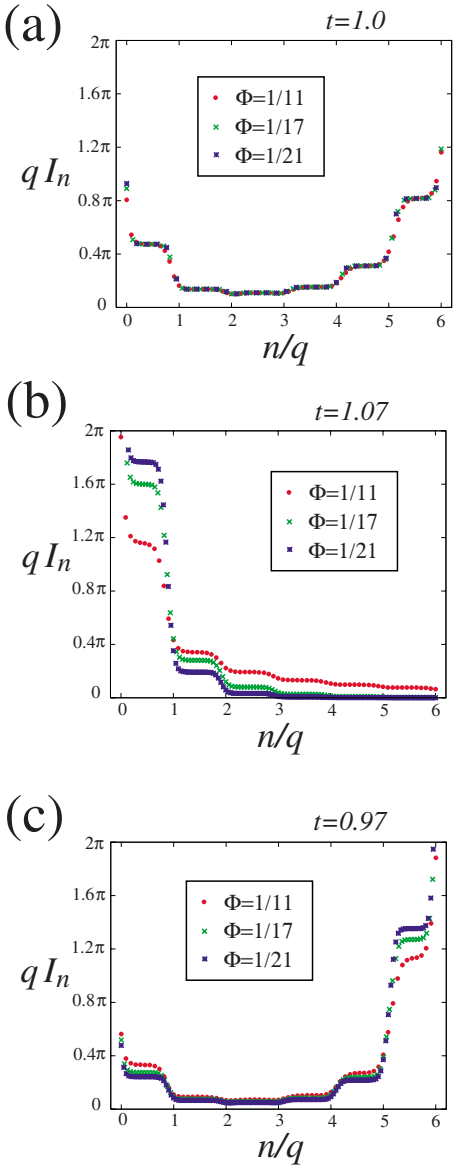

FIG. 16. (Color online) qI_n as a function of n/q for $\Phi=1/11$, 1/17, and 1/21. (a) $t=1.0$, (b) $t=1.07$, (c) $t=0.97$.

$$N_{\text{zigzag}} = d_{\text{zigzag}}\left(1-\frac{2}{t^{2q}}\right)-\frac{4}{t^{2q}}\int_{2\cos^{-1}(t^q/2)}^{\pi}\cos k_y dk_y$$

$$=2\left(\pi-2\cos^{-1}\frac{t^q}{2}\right)\left(1-\frac{2}{t^{2q}}\right)+\frac{4}{t^q}\sin\left(\cos^{-1}\frac{t^q}{2}\right),$$

$$N_{\text{bearded}} = d_{\text{bearded}}-\frac{t^{2q}}{2}\int_0^{2\cos^{-1}(t^q/2)}\frac{1}{\cos^2\left(\frac{k_y}{2}\right)}dk_y$$

$$=4\cos^{-1}\frac{t^q}{2}-2t^q\sin\left(\cos^{-1}\frac{t^q}{2}\right). \tag{91}$$

We also find that for $t=1$, N_{zigzag} and N_{bearded} are independent of Φ,

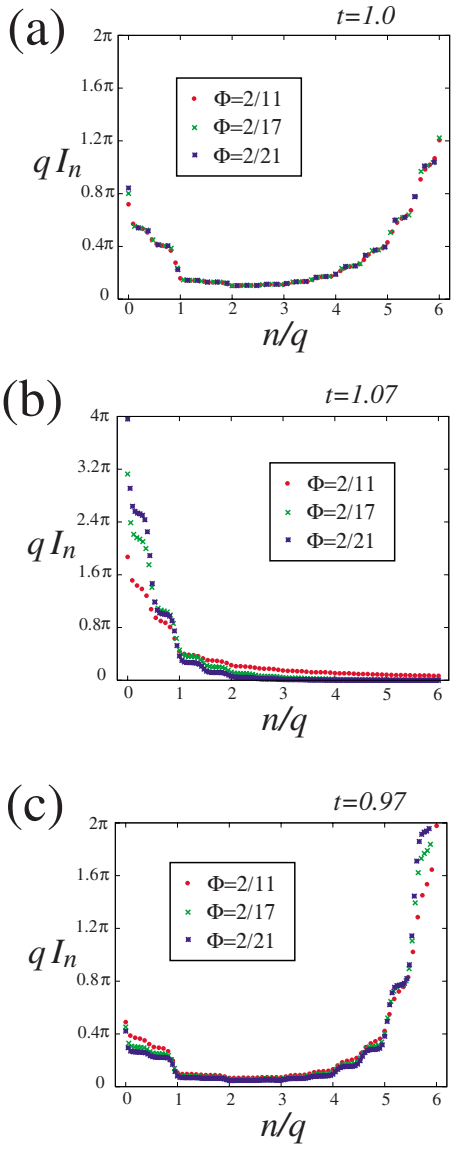

FIG. 17. (Color online) qI_n as a function of n/q for $\Phi=2/11$, 2/17, and 2/21. (a) $t=1.0$, (b) $t=1.07$, (c) $t=0.97$.

$$N_{\text{zigzag}} = 2\sqrt{3}-\frac{2\pi}{3},\quad N_{\text{bearded}} = \frac{4}{3}\pi-\sqrt{3}. \tag{92}$$

These formulas also show that a small anisotropy induces sudden changes in the edge states in a weak magnetic field: when q increases for a fixed $t>1$, N_{zigzag} increases toward 2π and N_{bearded} reaches zero at $q=\ln 2/\ln t$. And for a fixed $t<1$, N_{zigzag} goes to zero and N_{bearded} increases toward 2π as q increases. Thus in a weak magnetic field ($q\gg 1$), there are abrupt changes in N_{zigzag} and N_{bearded} at $t=1$.

In Figs. 16 and 17, we show scaled plots of I_n as a function of n/q. Here we have taken $L_x=6q$. Because of the normalization condition (83), I_n decreases as $\sim 1/L_x$ when L_x increases. To remove the artificial dependence on L_x, we plot qI_n instead of I_n. For $t=1$, qI_n's for different $\Phi(=p/q)$'s with the same p fall on a common curve.[22] However, for $t>1$, qI_n comes to be localized on q sites from the zigzag edges as Φ (with the same p) decreases. In contrast, for $t<1$, qI_n comes

TABLE II. Numerical data, N_{zigzag}, N_{bearded}, and analytical results, $N_{\text{zigzag}}^{(\text{A})}$, $N_{\text{bearded}}^{(\text{A})}$. (a) $t=1.0$ (b) $t=1.07$ (c) $t=0.97$. The relative discrepancies between numerical data and analytical results, $\delta_{\text{zigzag}}=|(N_{\text{zigzag}}^{(\text{A})}-N_{\text{zigzag}})/N_{\text{zigzag}}|$ and $\delta_{\text{bearded}}=|(N_{\text{bearded}}^{(\text{A})}-N_{\text{bearded}})/N_{\text{bearded}}|$, are also shown.

Φ	N_{zigzag}	N_{bearded}	$N_{\text{zigzag}}^{(\text{A})}$	$N_{\text{bearded}}^{(\text{A})}$	δ_{zigzag}	δ_{bearded}
			(a) $t=1.0$			
1/11	1.484	2.562			0.0770	0.0411
2/11	1.484	2.562			0.0770	0.0411
1/17	1.485	2.563	$2\sqrt{3}-\frac{2}{3}\pi$	$\frac{4}{3}\pi-\sqrt{3}$	0.0776	0.0415
2/17	1.485	2.563			0.0776	0.0415
1/21	1.486	2.563			0.0783	0.0415
2/21	1.486	2.563			0.0783	0.0415
			(b) $t=1.07$			
1/11	3.635	0.2336	3.447		0.0517	
2/11	3.635	0.2335			0.0517	
1/17	5.027	0.009609	5.024	0	0.000597	
2/17	5.027	0.009591			0.000597	
1/21	5.550	0.0007872	5.550		0.00	
2/21	5.550	0.0007847			0.00	
			(c) $t=0.97$			
1/11	1.040	3.553	0.9665	3.484	0.0707	0.0194
2/11	1.040	3.553			0.0707	0.0194
1/17	0.8618	3.992	0.8017	3.936	0.0697	0.0140
2/17	0.8618	3.992			0.0697	0.0140
1/21	0.7610	4.248	0.7083	4.198	0.0693	0.0118
2/21	0.7610	4.248			0.0693	0.0118

to be localized on q sites from the bearded edges as Φ (with the same p) decreases. In Table II, we also compare numerical data and analytical results presented above. With relative discrepancies less than 10%, they exhibit good agreements.

So far, we have assumed that $L_x \gg q$. When $L_x \lesssim q$, the above arguments cannot be justified. However, numerical calculations suggest that if $L_x \gg 1/\Phi$ $(pL_x \gg q)$, the particular edge states presented above appear again. In Fig. 18, we show the energy bands for $L_x=50$ and $\Phi=1001/5000(\sim 1/5)$, which are found to be indistinguishable from those for $\Phi=1/5$ (Fig. 14). It is also found that if the magnetic field decreases and $L_x \lesssim 1/\Phi$ is realized, then the energy bands approach those without a magnetic field, which is illustrated in Fig. 19.

VI. SUMMARY AND DISCUSSION

In this paper, we examined behavior of zero modes and a gap around zero energy for a tight-binding model on the anisotropic honeycomb lattice in a magnetic field, whose anisotropy is controlled by the hopping parameter t. It was found that zero modes exist for all (rational) Φ for $0<t\leq 1$, and a gap around zero energy opens by a tiny anisotropy for the graphene in a magnetic field. This is contrasted with the case for the square lattice, where zero modes always exist for all (rational) Φ when we change the ratio of the hopping parameters t_x/t_y.[35] For $1<t<2$, a gap around zero energy in a weak magnetic field behaves as a nonperturbative and exponential form as a function of the magnetic field. This nonanalytic behavior is naturally explained by tunneling effects between energy levels around two Dirac zero modes in the absence of a magnetic field. At $t=2$, the gap around zero energy in a weak magnetic field makes a

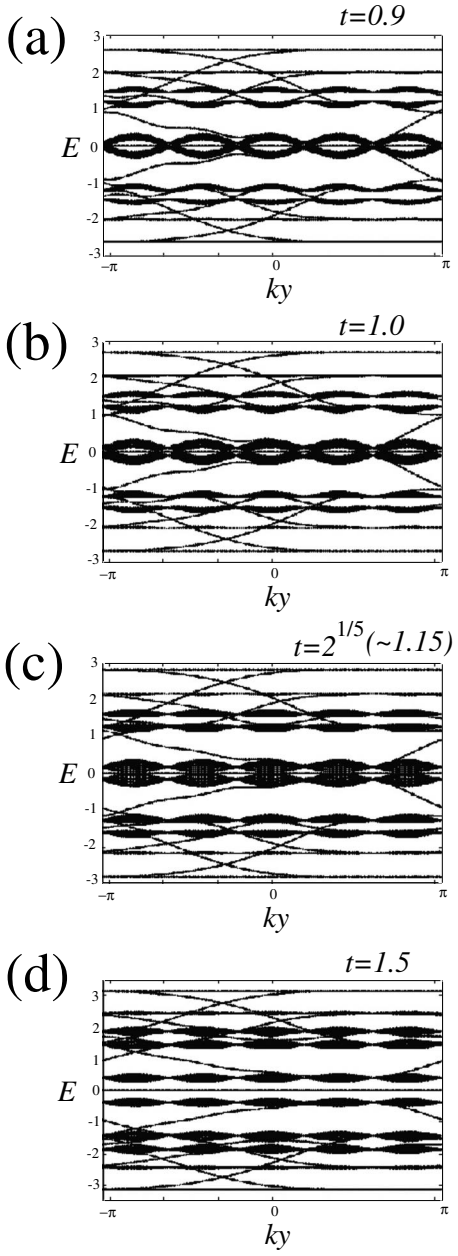

FIG. 18. Energy spectra of honeycomb lattices with zigzag and bearded edges for $\Phi=1001/5000(\sim 1/5)$ and $L_x=50$. (a) $t=0.9$, (b) $t=1.0$, (c) $t=2^{1/5}(\sim 1.15)$ (d) $t=1.5$.

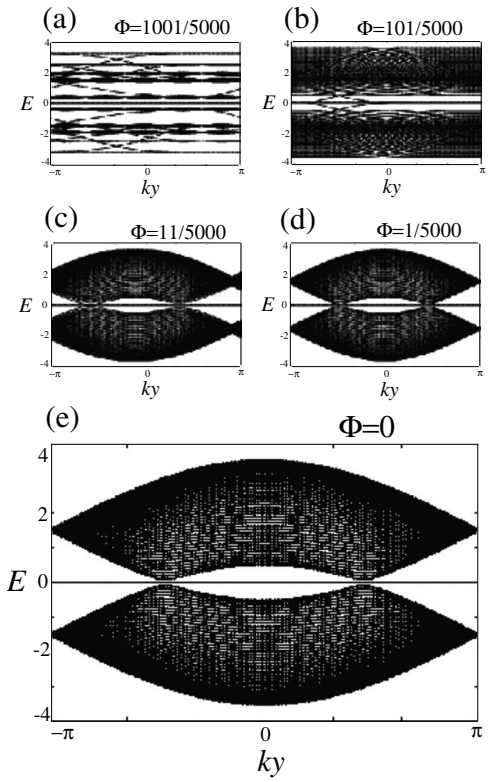

FIG. 19. Energy spectra of honeycomb lattices with zigzag and bearded edges for $t=1.5$ and $L_x=50$. (a) $\Phi=1001/5000$, (b) $\Phi=101/5000$, (c) $\Phi=11/5000$, (d) $\Phi=1/5000$. We also show energy bands in the absence of a magnetic field in (e).

transition from an exponential (nonperturbative) to a power-law (perturbative) behavior as a function of the magnetic field. In particular, an explicit form of the gap around zero energy near the transition point is obtained by the WKB method. For $t>2$, energy bands in a weak magnetic field show linear dependence on a magnetic field.

We also examined edge states with zero energy. The condition for the existence of zero energy edge states in a magnetic field is analytically derived. On the basis of the condition, it is found that the anisotropy of the hopping integrals induces abrupt changes in the number of zero energy edge states, which depend on the shapes of the edges sensitively.

Finally, we would like to discuss possible experimental realization of anisotropy of the hopping integrals. Recently, it was experimentally found that a reversible and controlled uniaxial strain can be produced in graphene.[36,37] Therefore, we can expect that a small anisotropy of the hopping integrals is realized by the uniaxial strain. On the other hand, in order to realize a large anisotropy such as $t\sim 2$, cold atoms in optical honeycomb lattices created by laser beams would serve as alternatives.[25] In these lattices, a large anisotropy could be induced and controlled by changing the intensities of the laser fields.[38] In addition, by using Raman processes induced by laser fields, effective magnetic fields can be generated in the optical lattice.[39]

Note added. Recently, we became aware of recent independent work which has some overlap with ours for $t\sim 2$.[40,41] We are grateful to G. Montambaux for pointing out these papers.

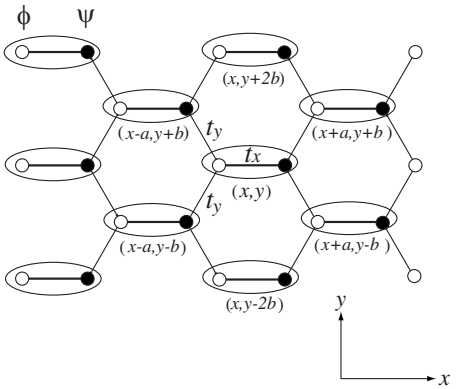

FIG. 20. A honeycomb lattice with a variable lattice spacing. If $a=\sqrt{3}b$, we have the hexagonal symmetry for each sublattice.

ACKNOWLEDGMENTS

This work was supported in part by Global COE Program "the Physical Sciences Frontier," MEXT, Japan for K.E. This work was also supported in part by NSF Grant No. DMR-05-41988 for B.I.H.

Appendix: Tight-binding model on a honeycomb lattice with a variable lattice spacing

In this appendix, we consider a honeycomb lattice with a variable lattice spacing shown in Fig. 20. The tight-binding equation in a magnetic field is given by

$$E\psi(x,y) = t_y[\phi(x+a,y-b) + e^{2i\pi(\Phi/a)x}\phi(x+a,y+b)] + t_x\phi(x,y),$$

$$E\phi(x,y) = t_y[\psi(x-a,y+b) + e^{-2i\pi(\Phi/a)(x-a)}\psi(x-a,y-b)] + t_x\psi(x,y), \tag{A1}$$

where a magnetic flux through a unit hexagon with an area of $S=2ab$ is given by $2\pi\Phi$. Let us write

$$x=na, \quad y=mb, \tag{A2}$$

then Eq. (A1) gives

$$E\psi(na,mb) = t_y\{\phi[(n+1)a,(m-1)b] + e^{2i\pi\Phi n}\phi[(n+1)a,(m+1)b]\} + t_x\phi(na,mb),$$

$$E\phi(na,mb) = t_y\{\psi[(n-1)a,(m+1)b] + e^{-2i\pi\Phi(n-1)}\psi[(n-1)a,(m-1)b]\} + t_x\psi(na,mb). \tag{A3}$$

Then, by writing $\psi_{n,m}=\psi(na,mb)$, $\phi_{n,m}=\phi(na,mb)$, and putting $t=t_x/t_y$, $t_y=1$, we obtain the tight-binding Eq. (1) from Eq. (A3).

When we have lattice spacings a and b in the x and y directions, respectively, as shown in Fig. 20, the momenta q_x and q_y in the x and y directions are related to k_x and k_y defined in Eq. (3) as

$$k_x = aq_x, \quad k_y = bq_y. \tag{A4}$$

Especially, for $a=\sqrt{3}b$, where each sublattice has the hexagonal symmetry, we have

$$k_x = aq_x, \quad k_y = \frac{a}{\sqrt{3}}q_y. \tag{A5}$$

Here, we mention the relation between the magnetic field B and the magnetic flux Φ. They are related as

$$BS = 2abB = 2\pi\Phi, \tag{A6}$$

that is,

$$B = \frac{\pi\Phi}{ab}. \tag{A7}$$

The tight-binding Eq. (1) corresponds to $a=b=1$, thus from Eq. (A7) B and Φ are related as

$$B = \pi\Phi. \tag{A8}$$

[1] K. S. Novoselov, A. K. Geim, S. V. Morozov, D. Jiang, M. I. Katsnelson, I. V. Grigorieva, S. V. Dubonos, and A. A. Firsov, Nature (London) **438**, 197 (2005).

[2] Y. Zhang, Y.-W. Tan, H. L. Stormer, and P. Kim, Nature (London) **438**, 201 (2005).

[3] M. L. Sadowski, G. Martinez, M. Potemski, C. Berger, and W. A. de Heer, Phys. Rev. Lett. **97**, 266405 (2006).

[4] Z. Jiang, E. A. Henriksen, L. C. Tung, Y.-J. Wang, M. E. Schwartz, M. Y. Han, P. Kim, and H. L. Stormer, Phys. Rev. Lett. **98**, 197403 (2007).

[5] R. S. Deacon, K. -C. Chuang, R. J. Nicholas, K. S. Novoselov, and A. K. Geim, Phys. Rev. B **76**, 081406(R) (2007).

[6] V. P. Gusynin and S. G. Sharapov, Phys. Rev. Lett. **95**, 146801 (2005).

[7] Y. Zheng and T. Ando, Phys. Rev. B **65**, 245420 (2002).

[8] N. M. R. Peres, F. Guinea, and A. H. Castro Neto, Phys. Rev. B **73**, 125411 (2006).

[9] M. Sato, D. Tobe, and M. Kohmoto, Phys. Rev. B **78**, 235322 (2008).

[10] D. J. Klein, Chem. Phys. Lett. **217**, 261 (1994).

[11] M. Fujita, K. Wakabayashi, K. Nakada, and K. Kusakabe, J. Phys. Soc. Jpn. **65**, 1920 (1996).

[12] K. Nakada, M. Fujita, G. Dresselhaus, and M. S. Dresselhaus, Phys. Rev. B **54**, 17954 (1996).

[13] K. Wakabayashi, M. Fujita, H. Ajiki, and M. Sigrist, Phys. Rev. B **59**, 8271 (1999).

[14] K. Kusakabe and Y. Takagi, Mol. Cryst. Liq. Cryst. **387**, 7 (2002).

[15] S. Ryu and Y. Hatsugai, Phys. Rev. Lett. **89**, 077002 (2002).

[16] M. Ezawa, Phys. Rev. B **73**, 045432 (2006).

[17] B. A. Bernevig, T. L. Hughes, S.-C. Zhang, H.-D. Chen, and C. Wu, Int. J. Mod. Phys. B **20**, 3257 (2006).

[18] B. A. Bernevig, T. L. Hughes, and S.-C. Zhang, Solid State Commun. **143**, 20 (2007).

[19] Y. Hatsugai, T. Fukui, and H. Aoki, Phys. Rev. B **74**, 205414 (2006).

[20] H. Aoki, T. Fukui, and Y. Hatsugai, Int. J. Mod. Phys. B **21**, 1133 (2007).

[21] M. Arikawa, Y. Hatsugai, and H. Aoki, Phys. Rev. B **78**, 205401 (2008).

[22] M. Arikawa, Y. Hatsugai, and H. Aoki, J. Phys.: Conf. Ser. **150**, 022003 (2009).

[23] Y. Hasegawa and M. Kohmoto, Phys. Rev. B **74**, 155415 (2006).

[24] Y. Hasegawa, R. Konno, H. Nakano, and M. Kohmoto, Phys. Rev. B **74**, 033413 (2006).

[25] P. Dietl, F. Piéchon, and G. Montambaux, Phys. Rev. Lett. **100**, 236405 (2008).

[26] M. Kohmoto, Int. J. Mod. Phys. B **23**, 3113 (2009).

[27] V. M. Pereira, A. H. Castro Neto, and N. M. R. Peres, Phys. Rev. B **80**, 045401 (2009).

[28] M. Kohmoto and Y. Hasegawa, Phys. Rev. B **76**, 205402 (2007).

[29] E. Witten, Nucl. Phys. B **188**, 513 (1981).

[30] E. Witten, Nucl. Phys. B **202**, 253 (1982).

[31] R. Rammal, J. Phys. (Paris) **46**, 1345 (1985).

[32] Note that, from the definition (3), k_x and k_y have different units of length from each other in our convention. See Eqs. (A4) and (A5) in Appendix.

[33] H. Aoyama, H. Kikuchi, I. Okouchi, M. Sato, and S. Wada, Nucl. Phys. B **553**, 644 (1999).

[34] I. S. Gradshteyn and I. M. Ryzhik, *Tables of Integrals, Series, and Products*, 7th ed. (Academic press, New York, 2007).

[35] M. Kohmoto, Phys. Rev. B **39**, 11943 (1989).

[36] Z. H. Ni, H. M. Wang, Y. Ma, J. Kasim, Y. H. Wu, and Z. X. Shen, ACS Nano **2**, 1033 (2008).

[37] Z. H. Ni, T. Yu, Y. H. Lu, Y. Y. Wang, Y. P. Feng, and Z. X. Shen, ACS Nano **2**, 2301 (2008); **3**, 483 (2009).

[38] S.-L. Zhu, B. Wang, and L.-M. Duan, Phys. Rev. Lett. **98**, 260402 (2007).

[39] D. Jaksch and P. Zoller, New J. Phys. **5**, 56 (2003).

[40] G. Montambaux, F. Piéchon, J.-N. Fuchs, and M. O. Goerbig, arXiv:0904.2117 (unpublished).

[41] G. Montambaux, F. Piéchon, J.-N. Fuchs, and M. O. Goerbig, arXiv:0907.0500 (unpublished).